Automatic Shape Optimization of Patient-Specific Tissue Engineered Vascular Grafts for Aortic Coarctation

Xiaolong Liu[1], Seda Aslan[1], Rachel Hess[1], Paige Mass[2], Laura Olivieri[2], Yue-Hin Loke[2],
Narutoshi Hibino[3], Mark Fuge[1] and Axel Krieger[1]

Abstract—This paper proposes a computational framework for automatically optimizing the shapes of patient-specific tissue engineered vascular grafts. We demonstrate a proof-of-concept design optimization for aortic coarctation repair. The computational framework consists of three main components including 1) a free-form deformation technique exploring graft geometries, 2) high-fidelity computational fluid dynamics simulations for collecting data on the effects of design parameters on objective function values like energy loss, and 3) employing machine learning methods (Gaussian Processes) to develop a surrogate model for predicting results of high-fidelity simulations. The globally optimal design parameters are then computed by multi-start conjugate gradient optimization on the surrogate model. In the experiment, we investigate the correlation among the design parameters and the objective function values. Our results achieve a 30% reduction in blood flow energy loss compared to the original coarctation by optimizing the aortic geometry.

I. INTRODUCTION

Among the leading causes of newborn death, congenital heart disease (CHD) affects nearly 40,000 infants in the US per year with approximately 25% of neonates born with CHD requiring invasive or other potentially lifesaving treatments [1]. Aortic arch anomalies such as aortic coarctation and hypoplasia often require early surgical intervention to preserve normal systemic perfusion [2].

The current surgical repair techniques of aortic coarctation include 1) resection with end-to-end anastomosis, 2) patch aortoplasty, 3) interposition grafts, and 4) subclavian flap aortoplasty. In cases of significant associated arch hypoplasia, an aortic arch reconstruction may be required, which combines several of the techniques above [3], [4]. The current techniques can result distortion of the aortic arch shape, and is limited by the available synthetic materials such as polytetrafluoroethylene (PTFE) or polyester (Dacron®) which do not grow with the child and thus require revision or replacement [5]. In addition to poor growth, these synthetic materials also demonstrate calcification and stenosis, requiring multiple interventions in the long term that hinder their application in pediatric aorta surgery. Biocompatible materials, including autografts and allografts, works well although they have a limited availability and can be prone to dilation over time [6].

[1] X. Liu, S. Aslan, R. Hess, M. Fuge, and A. Krieger are with the Department of Mechanical Engineering, University of Maryland, College Park, MD, USA (e-mail: xlongliu@umd.edu).

[2] P. Mass Y. Loke and L. Olivieri are with Sheikh Zayed Institute for Pediatric Surgical Innovation, Children's National Hospital, Washington DC, USA

[3] N. Hibino is with Department of Cardiac Surgery, The University of Chicago Medicine, Chicago, IL, USA

Tissue engineered vascular grafts (TEVGs) offer a promising strategy for overcoming such complications. Using an FDA approved biodegradable scaffold, such as poly-L-lactide (PLLA) and poly-e-caprolactone (PCL), the patient's own cells can proliferate and provide physiologic functionality and growth over time [7]. To create TEVGs with custom shapes, electrospun nanofibers can be deposited on a 3D printed stainless steel mandrel [8]. For example, our work demonstrated feasible 3D-printed TEVGs in venous circulation using a sheep model [9]. The feasibility of customizing the shapes of TEVGs opens the door to designing patient-specific grafts that achieve optimal patient outcomes during aorta repair. Surgical intuition can be combined with computational predictions of hemodynamics to achieve an optimized, durable, patient-specific design for aortic arch repair.

Our research objective is to develop a computational framework for automatically designing optimal shapes of patient-specific TEVGs for aorta surgery. In our prior research [10], [11], we have investigated manual design optimization of patient-specific graft geometry by using computational fluid dynamics (CFD) and computer-aided design (CAD) software. Custom design tools for graft geometry manipulation were developed by other research groups for the ease of manual design process [12], [13]. Nonetheless, considering manual design optimization involves time consuming trial-and-error process to achieve suboptimal hemodynamic performance, gradient-based and derivative-free design optimization algorithms in combination with CFD analysis have been used to optimize 2-D/3-D ideal models of coronary artery by-pass grafts (CABGs) [14], [15], [16]. By using the ideal model assumption, shape parameterization and optimization of graft geometry can be significantly simplified. Different from CABGs, aortic grafts cannot be treated by using ideal models due to the variety of aorta shapes. Therefore, automatic design optimization of patient-specific aortic graft for clinical needs is still an open problem.

In this paper, we demonstrate a computational framework for automatically optimizing the shape of patient-specific tissue engineered vascular grafts. We apply this computational framework to a case of aortic coarctation for proof-of-concept. By controlling a set of design parameters to deform a cylindrical lattice applied on a patient's native aorta model, various geometric shapes are generated for computing values of the objective function by CFD simulation. Instead of using commercial CFD software, we employ an open-source CFD solver (OpenFOAM) [17] which is seamlessly integrated in our computational framework. Based on the observation data from CFD simulation, the hemodynamic surrogate model for each
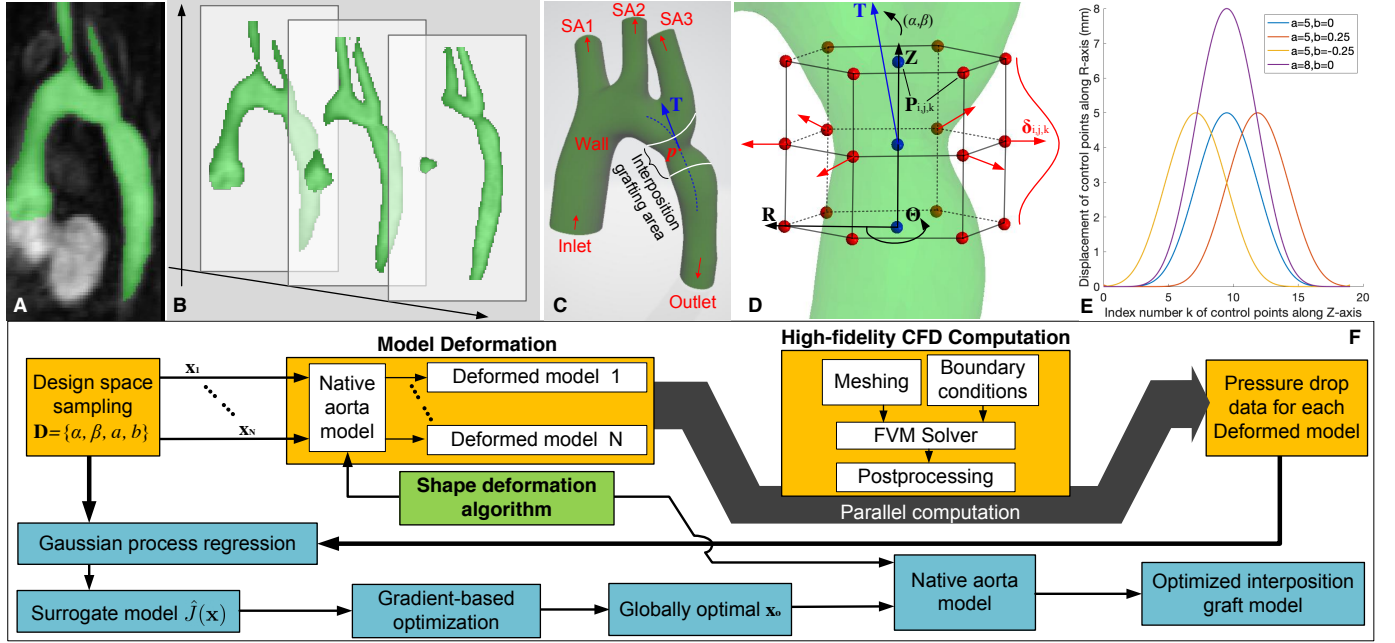
Fig. 1. Illustration of aorta model preparation and computational framework of design optimization. (A) 3D contrast-enhanced magnetic resonance angiography (MRA) of aorta. (B) Slices of the MRA dataset for 3D aorta model reconstruction. (C) Region of interest for design optimization (red circle) and boundaries for numerical computation. (D) Illustration of the shape deformation method. (E) Displacement patterns of control points by varying a and b in $\boldsymbol{\delta}_{i,j,k}$. (F) Computational framework for automatic design optimization.

patient's aorta is trained by using Gaussian process regression. The globally optimal design parameters can be found by running a multi-start conjugate gradient optimization on the surrogate model for computing the final geometric shapes of the TEVGs. The primary contributions of this paper include: 1) demonstration of an automatic optimization pipeline for designing TEVGs; 2) an effective freeform deformation method for representing and exploring the shape of aortic grafts; and 3) online training and optimizing the hemodynamic surrogate model to identify the optimal design parameters.

II. METHOD

Fig. 1 shows the preparation of a patient's native aorta model and the computational strategy for design optimization. Contrast-enhanced magnetic resonance angiography (MRA) data as shown in Fig. 1A was used to build a 3D virtual model of the aorta through a segmentation process, in which a sequence of spatially distributed slices of MRA dataset were created as shown in Fig. 1B. The shape deformation method (Fig. 1D) is applied on the smoothed 3D aorta model (Fig. 1C) to explore optimal shapes of the coarctation area.

The objective of this proof-of-concept design optimization is to minimize the energy loss J of blood flow between the inlet and the outlet shown in Fig. 1C by deforming the shape of the coarctation area. The design space $\mathbf{D}$ includes design parameters to control deformation of the cylinder lattice and subsequently control the shape of the aorta model. Fig. 1F demonstrates the computational framework of automatic design optimization. A computationally low-cost Gaussian process surrogate model is developed to replace the high-fidelity CFD for approximating the objective function $J(\mathbf{x})$. The

training data of the surrogate model are obtained by running a limited number of high-fidelity CFD simulation as shown in the yellow blocks of Fig. 1F. By applying gradient-based optimization on the surrogate model, the globally optimal design parameters $\mathbf{x}_o$ can be found. The optimal shape of graft for the area of aortic coarctation is restored by feeding $\mathbf{x}_o$ to the shape deformation algorithm. In the following, we discuss the major components of our method in detail.

A. Graft Shape Deformation and Parameterization

The shape deformation algorithm for graft optimization in this paper is based on free-form deformation (FFD) [18]. The main idea of FFD is to deform an object by warping the space that contains the object. We construct a cylinder lattice as shown in Fig. 1D to cover the space where the coarcation is located. Given a set of arbitrary global coordinates (r, θ, z) in the space, the reference coordinates $(\hat{r}, \hat{\theta}, \hat{z})$ of the unit trivariate space can be calculated by $\hat{r} = r/|\mathbf{R}|, \hat{\theta} = \theta/|\mathbf{\Theta}|, \hat{z} = z/|\mathbf{Z}|$.

The warping of the space is formulated in the mapping function $\mathbf{X}_m(\hat{r}, \hat{\theta}, \hat{z})$ with nodes $\mathbf{P}_{i,j,k}$ on the lattice as control points.

$$\mathbf{X}_m = \sum_{i=0}^{n_r} \sum_{j=0}^{n_\theta} \sum_{k=0}^{n_z} B_{i,n_r}(\hat{r}) B_{j,n_\theta}(\hat{\theta}) B_{k,n_z}(\hat{z}) \left(\mathbf{P}_{i,j,k} + \boldsymbol{\delta}_{i,j,k} \right), \quad (1)$$

where $r = i/n_r, \theta = j/n_\theta, z = k/n_z$. n_r, n_θ and n_z are the number the control points in directions of $\mathbf{R}, \mathbf{\Theta}$ and $\mathbf{Z}$ without counting the local origin point. $B_{i,n_r}(\hat{r}), B_{j,n_\theta}(\hat{\theta})$ and $B_{k,n_z}(\hat{z})$ are the n_r-order, n_θ-order and n_z-order Bernstein basis polynomial functions. We introduce a vector parameter $\boldsymbol{\delta}_{i,j,k}$ with dimensions of $3 \times (n_r + 1) \times (n_\theta + 1) \times (n_z + 1)$ for adding a spatial offset on $\mathbf{P}_{i,j,k}$.

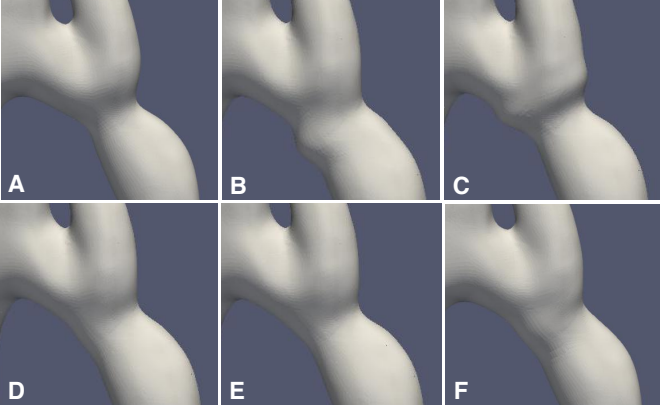The coordinates of $\mathbf{P_{i,j,k}}$ are represented as

Fig. 2. Illustration of the shape deformation algorithm with randomly sampled design parameters $\mathbf{x} = (\alpha, \beta, a, b)$. (A) Native model $\mathbf{x}_A = (0°, 0°, 0\,\mathrm{mm}, 0)$. (B) $\mathbf{x}_B = (27.6°, 5.3°, 7\,\mathrm{mm}, -0.24)$. (C) $\mathbf{x}_C = (75.4°, 9.1°, 5\,\mathrm{mm}, 0.24)$. (D) $\mathbf{x}_D = (304.6°, 3.7°, 3.5\,\mathrm{mm}, -0.1)$. (E) $\mathbf{x}_E = (54.2°, 9.7°, 2.1\,\mathrm{mm}, 0.04)$. (F) $\mathbf{x}_F = (201.3°, 20.8°, 4.5\,\mathrm{mm}, -0.15)$.

$$\mathbf{P}_{i,j,k} = \mathbf{X}_0 + \frac{i}{n_r}\mathbf{R} + \frac{j}{n_\theta}\mathbf{\Theta} + \frac{k}{n_z}\mathbf{Z}, \qquad (2)$$

where $0 \le i \le n_r, 0 \le j \le n_\theta, 0 \le i \le n_z$. In this study, we set $n_r = 1, n_\theta = 14, n_z = 20, |\mathbf{R}| = 18\,\mathrm{mm}, |\mathbf{\Theta}| = 2\pi$ and $|\mathbf{Z}| = 20\,\mathrm{mm}$ for creating a cylinder space to contain the segment of coarctation.

To efficiently explore the geometry deformation at the coarctation region, our strategy is to move the control points in groups instead of controlling all the dimensions of $\boldsymbol{\delta}_{i,j,k}$ individually. Considering the shape of the coarctation area, an intuitive shape exploration is to stent this area. Therefore, in this paper we design a deformation function in (3) to move the control points radially away from the centerline $\mathbf{Z}$ of the cylinder lattice.

$$\delta_{1,j,k} = a\left(1 - \left(\frac{2k}{n_z} - 1 - b\right)^2\right)^8 \qquad (3)$$

The profiles of (3) are illustrated in Fig. 1E. This function is only dependent on node index k in $\mathbf{Z}$ direction, applies to the control points on the cylinder wall (red nodes in Fig. 1D), and moves the control points in $\mathbf{R}$ direction. We set $\delta_{0,j,k}$ to zero for keeping the blue nodes (Fig. 1D) along the centerline unmovable. The parameters a and b are used to adjust the peak magnitude and offset for various patterns of deformation.

In order to provide more freedom on exploring the shape deformation, we introduce two additional parameters α and β, which control the direction of the cylinder lattice's $\mathbf{Z}$-axis around $\mathbf{T}$ shown in Fig. 1C-D. $\mathbf{T}$ is a tangent vector of the aorta model's centerline at the point $\boldsymbol{p}_o$.

Fig. 2 demonstrates shape deformation of the aorta model by controlling the design parameters $\mathbf{x} = (\alpha, \beta, a, b) \in \mathbf{D} \subset \mathbb{R}^4$. The design space $\mathbf{D}$ in this study is set as $a \in [0, 10\,\mathrm{mm}]$, $b \in [-0.25, 0.25]$, $\alpha \in [0°, 360°]$ and $\beta \in [0°, 10°]$ according to the specific model tested in this paper. The following task is to find a set of design parameters that yield the minimized energy loss of blood flow.

B. Gaussian Process Surrogate Model and Optimization

The energy loss of blood flow is represented by inlet-outlet pressure drop $J(\mathbf{x})$ for each deformed aorta model

in this proof-of-concept study. The measurement of $J(\mathbf{x})$ involves running computationally expensive CFD simulation that prohibits searching for all different combinations of design parameters. An alternative solution for this task is to train a surrogate model $\hat{J}(\mathbf{x})$ to approximate the exact objective function $J(\mathbf{x})$ by using Gaussian process regression:

$$\hat{J}(\mathbf{x}) = \hat{\gamma} + \mathbf{c}^T(\mathbf{x})\mathbf{C}^{-1}(\mathbf{J} - \hat{\gamma}\mathbf{f}), \qquad (4)$$

where $\mathbf{C}$ represents the covariance matrix with the kernel function modeled as

$$C(\mathbf{x}^i, \mathbf{x}^j) = \exp\left(-\sum_{s=1}^{n_s} \theta_s |\mathbf{x}^i - \mathbf{x}^j|^2\right). \qquad (5)$$

$\mathbf{c}(\mathbf{x})$ is the covariance vector

$$\mathbf{c}(\mathbf{x}) = [C(\mathbf{x}, \mathbf{x}^1), ..., C(\mathbf{x}, \mathbf{x}^{n_s})]. \qquad (6)$$

θ_s denotes correlation parameters. $\mathbf{J}$ represents the vector of n_s observed pressure drops ($n_s = 50$ in this study) which are obtained by using the method in Section II-C. $\mathbf{x}^i$ ($i = 1, ..., n_s$) represents the sampled design parameters by using Latin hypercube sampling (LHS) method. $\mathbf{f}$ is a unity vector with a dimension of $1 \times n_s$. $\hat{\gamma}$ is obtained by using generalized least squares as

$$\hat{\gamma} = (\mathbf{f}^T\mathbf{C}^{-1}\mathbf{f})^{-1}\mathbf{f}^T\mathbf{C}^{-1}\mathbf{J}. \qquad (7)$$

The objective of design optimization is to find $\mathbf{x}_o$ for minimizing $\hat{J}(\mathbf{x})$, which is mathematically described in (8).

$$\mathbf{x}_o = \underset{\mathbf{x} \in \mathbf{D}}{\arg\min}\, \hat{J}(\mathbf{x}) \qquad (8)$$

In order to search globally optimal design parameters, we employ a multi-start conjugate gradient method on $\hat{J}(\mathbf{x})$ by sampling sets of design parameters in the design space $\mathbf{D}$. Then we use $\mathbf{x}_o$ as the input of the shape deformation algorithm to apply on the native model of aorta. An optimized TEVG can thus be manufactured by 3D electrospinning based on the shape of the optimally deformed model.

C. High-Fidelity CFD Computation

The hemodynamics of the aorta is governed by the Navier Stokes equation and the continuity equation in (9) and (10) based on the following assumptions for ensuring reasonable computation time: 1) blood was modeled as Newtonian, incompressible laminar flow with constant viscosity of $\mu = 3.5 \times 10^{-3}\,\mathrm{Pa} \cdot \mathrm{s}$ and a density of $\rho = 1.06 \times 10^3\,\mathrm{kg} \cdot \mathrm{m}^{-3}$, 2) the aorta geometry was modeled with rigid walls.

$$\boldsymbol{u} \cdot \nabla \boldsymbol{u} + \frac{\nabla p}{\rho} - \nu \nabla^2 \boldsymbol{u} = 0 \qquad (9)$$

$$\nabla \cdot (\rho \boldsymbol{u}) = 0 \qquad (10)$$

In equations (9) and (10), $\boldsymbol{u}$ is the fluid velocity vector, p is the velocity pressure, and $\nu = \mu/\rho$ is the kinematic viscosity. As illustrated in Fig. 1C, the boundary conditions of the inlet (peak flow rate $0.96\,\mathrm{m} \cdot \mathrm{s}^{-1}$), outlet (pressure $9119.1\,\mathrm{Pa}$), SA1 (mass flow rate $0.087\,\mathrm{kg} \cdot \mathrm{s}^{-1}$), SA2 (mass flow rate $0.048\,\mathrm{kg} \cdot \mathrm{s}^{-1}$), and SA3 (mass flow rate $0.057\,\mathrm{kg} \cdot \mathrm{s}^{-1}$) were measured by MRI and invasive cardiac catheterization. The blood flow velocities at the aorta wall were assumed as zero.

To solve the velocity field and the pressure field in the computation domain, we employ OpenFOAM software package
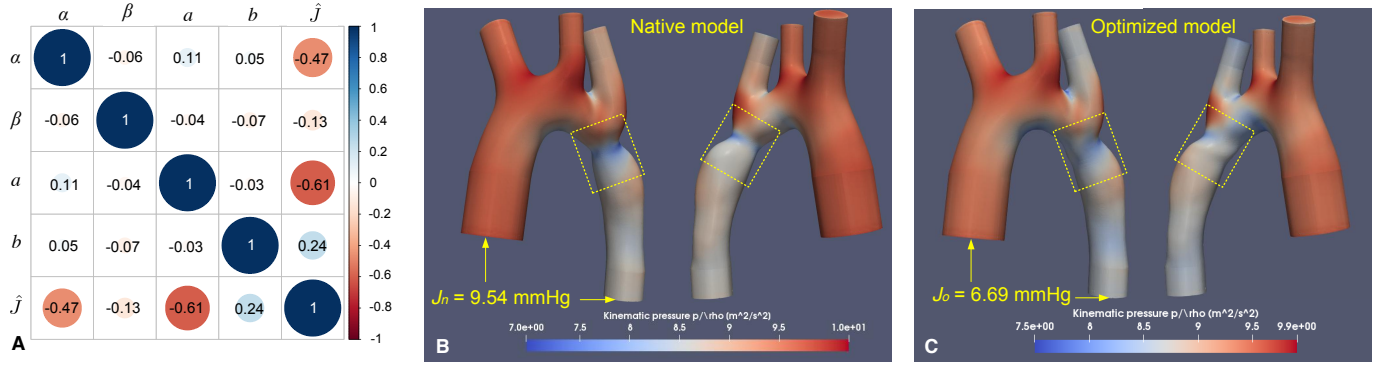
Fig. 3. Design optimization results. (A) Correlation matrix of design parameters (α, β, a, b) and pressure drop $\hat{J}$. (B) Pressure field distribution on the native aortic model. (C) Pressure field distribution on the optimized aortic model.

TABLE I
SELECTED 5 RESULTS OF MULTI-START OPTIMIZATION

	$\alpha(°)$	$\beta(°)$	$a(mm)$	b	$\hat{J}$ (mmHg)
1	222.43	4.56	4.08	-0.14	6.65
2	296.21	3.80	4.27	-0.07	6.71
3	241.84	5.06	4.12	-0.15	6.69
4	136.33	2.46	4.07	-0.14	6.68
5	359.41	4.42	4.42	-0.11	6.67

for meshing deformed aorta models (using snappyHexMesh mesher), solving (9) and (10) (using SimpleFoam solver), and extracting the inlet-outlet pressure drop J from the computed numerical results. The computational framework proposed in this paper supports parallel computation of the high-fidelity simulation for different deformed models, which can significantly reduce the total computation time.

III. RESULTS

A. Configuration and Computation Performance

The proposed computational framework of design optimization was written in C++ programming language, and run on a PC with the operating system of Ubuntu 18.04 LTS. The PC is with the configuration of Intel® Core™ i9-9900 CPU @3.10GHz and 32GB random-access memory.

The total computation time of the automatic optimization shown in Fig. 1F mainly depends on the number of computing cores for parallel computation (8 cores were used for this work), the number of high-fidelity CFD observation for training the surrogate model ($n_s = 50$), the number of mesh cells for each deformed model (about 0.5 million), the type of blood flow for CFD computation (laminar flow), and the dimension of design space $\mathbf{D}$ ($\mathbf{D} \subset \mathbb{R}^4$). In this work, it took about 3 hours and 20 minutes to complete the computation of design optimization.

B. Optimization Results

For searching the globally optimal design parameters, we sampled 20 sets of design parameters as the initial guesses for multi-start optimization on $\hat{J}$. Table I shows the optimized design parameters that yield 5 smallest $\hat{J}$ values. The optimized $\hat{J}$ falls in the short range from $6.65\,\mathrm{mmHg}$ to $6.71\,\mathrm{mmHg}$. To investigate the correlations among $\hat{J}$ and the design parameters

(α, β, a, b), we illustrate the correlation matrix in Fig. 3A. The cold colors represent negative correlation and the warm colors represent positive correlation. The numbers shown in the grid are the correlation coefficients. The data show α, β and a have negative correlations with $\hat{J}$, while b has positive correlation with $\hat{J}$. The design parameters α and a show stronger correlations with $\hat{J}$ than β and b.

Fig. 3B and Fig. 3C show the anterior and posterior coronal views of the native and optimized aorta models. We demonstrate the comparison of pressure field distribution for the native and optimized models. The optimized model was generated by using the design parameters in the first row of Table I. The deformation areas are highlighted in the yellow rectangles. The pressure field maps are represented by using kinematic pressure p/ρ with the unit of $\mathrm{m}^2 \cdot \mathrm{s}^{-2}$. We extracted the inlet-outlet pressure drops and converted kinematic pressure $\mathrm{m}^2 \cdot \mathrm{s}^{-2}$ to the clinically relevant pressure unit mmHg as $J_n = 9.54\,\mathrm{mmHg}$ and $J_o = 6.69\,\mathrm{mmHg}$ respectively. The results show about 30% energy loss reduction of blood flow in aorta by optimizing the aortic geometry at the coractation area.

Although significant improvement in energy loss was achieved in the optimized aorta graft, we can see that the coarctation was not completely fixed in Fig. 3C. We think the design space dimension used in this paper should be further increased by reformulating (3) to gain more freedom for exploring the remaining coarctation area, which will be conducted in our future study.

IV. CONCLUSION

This paper provided an initial evidence to demonstrate the effectiveness of our automatic shape optimization method for TEVG design. We proposed a shape deformation method with a set of design parameters to explore optimal graft shapes. To identify the optimal design parameters, we optimized a Gaussian process surrogate model, which is generated by using a set of observation data from high-fidelity CFD simulation. The optimization results showed about 30% energy loss reduction of blood flow in the optimized aorta model. According the preliminary results, we found using four design parameters for the graft shape exploration was unable to fully remove

the coarctation area. An improvement on the dimension of the design space is needed.

In addition, the laminar flow assumption used in this paper simplified the numerical computation of (9) and (10) to ensure reasonable computation time while still capable of capturing important fluid dynamic characteristics. But the Reynolds number of blood flow in aorta is typically greater than 2100 that suggests turbulent flow. In the future study, we plan to investigate if the different assumptions result in significant differences of optimized grafts.

REFERENCES

[1] Julien I.E Hoffman and Samuel Kaplan. The incidence of congenital heart disease. *Journal of the American College of Cardiology*, 39(12):1890 – 1900, 2002.

[2] Dijkema EJ, Leiner T, and Grotenhuis HB. Correction: Diagnosis, imaging and clinical management of aortic coarctation. *Heart*, 105(14):1148–1155, 2017.

[3] Suradi H and Hijazi ZM. Current management of coarctation of the aorta. *Glob Cardiol Sci Pract.*, 4:44, 2015.

[4] LeMaire SA, Weldon SA, and Coselli JS. Total aortic arch replacement: current approach using the trifurcated graft technique. *Ann Cardiothorac Surg*, 2(3):347–352, 2013.

[5] Stephanie Roll and et al. Jacqueline Müller-Nordhorn. Dacron$^{\circledR}$ vs. PTFE as bypass materials in peripheral vascular surgery – systematic review and meta-analysis. *BMC Surgery*, 8:22 – 22, 2008.

[6] Steven G. Wise, Michael J. Byrom, Anna Waterhouse, Paul G. Bannon, Martin K.C. Ng, and Anthony S. Weiss. A multilayered synthetic human elastin/polycaprolactone hybrid vascular graft with tailored mechanical properties. *Acta Biomaterialia*, 7(1):295 – 303, 2011.

[7] Samand Pashneh-Tala, Sheila MacNeil, and Frederik Claeyssens. The tissue-engineered vascular graft—past, present, and future. In *Tissue engineering. Part B, Reviews*, 2015.

[8] Anwarul Hasan, Adnan Memic, and et al. Nasim Annabi. Electrospun scaffolds for tissue engineering of vascular grafts. *Acta Biomaterialia*, 10(1):11 – 25, 2014.

[9] Takuma Fukunishi, Cameron Best, and et al. Sugiura, Tadahisa. Preclinical study of patient-specific cell-free nanofiber tissue engineered vascular grafts using three-dimensional printing in a sheep model. *The Journal of Thoracic and Cardiovascular Surgery*, 153(4):924–932, 2017.

[10] Siallagan D, Loke YH, and et al. Olivieri L. Virtual surgical planning, flow simulation, and 3-dimensional electrospinning of patient-specific grafts to optimize fontan hemodynamics. *J Thorac Cardiovasc Surg.*, 155(4):1734–1742, 2018.

[11] S. Aslan, Y. Loke, P. Mass, and et al. K. Nelson. Design and simulation of patient-specific tissue-engineered bifurcated right ventricle-pulmonary artery grafts using computational fluid dynamics. In *2019 IEEE 19th International Conference on Bioinformatics and Bioengineering (BIBE)*, pages 1012–1018, 2019.

[12] Kerem Pekkan, Brian Whited, Kirk Kanter, and et al. Shiva Sharma. Patient-specific surgical planning and hemodynamic computational fluid dynamics optimization through free-form haptic anatomy editing tool (SURGEM). *Medical and Biological Engineering and Computing*, 46(11):1139–1152, 2008.

[13] Mark Luffel, Mukul Sati, and et al. Jarek Rossignac. SURGEM: A solid modeling tool for planning and optimizing pediatric heart surgeries. *Computer-Aided Design*, 70:3 – 12, 2016.

[14] Alison L. Marsden, Jeffrey A. Feinstein, and Charles A. Taylor. A computational framework for derivative-free optimization of cardiovascular geometries. *Computer Methods in Applied Mechanics and Engineering*, 197(21):1890 – 1905, 2008.

[15] Onur Dur, Sinan Tolga Coskun, and et al. Coskun, Kasim Oguz. Computer-aided patient-specific coronary artery graft design improvements using cfd coupled shape optimizer. *Cardiovascular Engineering and Technology*, 2(1):35–47, 2011.

[16] Alfio Quarteroni and Gianluigi Rozza. Optimal control and shape optimization of aorto-coronaric bypass anastomoses. *Mathematical Models and Methods in Applied Sciences*, 13(12):1801–1823, 2003.

[17] Open-source Field Operation And Manipulation (OpenFOAM). https://openfoam.org/version/6/. Accessed: 2019-08-20.

[18] Sabine Coquillart. Extended free-form deformation: A sculpting tool for 3d geometric modeling. In *Proceedings of the 17th Annual Conference on Computer Graphics and Interactive Techniques*, SIGGRAPH '90, page 187–196, 1990.